Supplementary information for

Unveiling Anionic Migration Mechanisms Governed by Mixed-Anion Chemistry in Melilite Oxyfluorides

Lijia Zhou[1,#], Li Yang[1,#], Aydar Rakhmatullin[2], Shipeng Geng[1], Xiaoyan Yang[1,*], Mathieu Allix[2], Jiazheng Hao[3], Lunhua He[3], Mingxue Tang[4], Zewei Quan[5], Xiaojun Kuang[1,*]

1. *Guangxi Key Laboratory of Electrochemical and Magneto-chemical Functional Materials, College of Chemistry and Bioengineering, Guilin University of Technology, Guilin 541006, P. R. China*
2. *CEMHTI-CNRS, 1D avenue de la Recherche Scientifique, CS90055 45071 Orleans cedex 2, France*
3. *Spallation Neutron Source Science Center, Dongguan 523803, P. R. China*
4. *School of Materials Science and Engineering, University of Science and Technology Beijing, Beijing 100083, P. R. China*
5. *Department of Chemistry, Southern University of Science and Technology (SUSTech), Shenzhen, Guangdong 518055, P. R. China*

*E-mail: yangxy@glut.edu.cn (X.Y.) ; kuangxj@glut.edu.cn (X.K.)

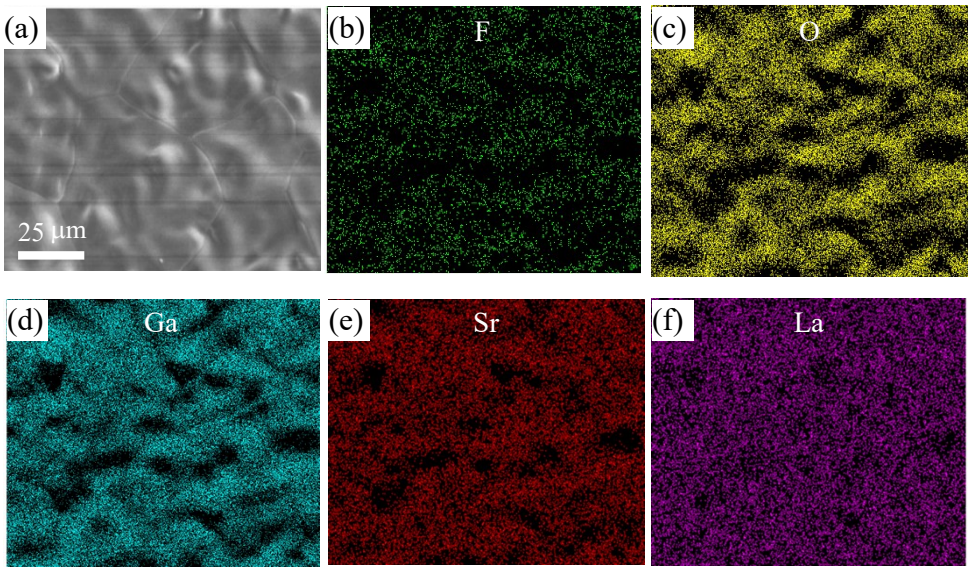

Figure S1. (a) SEM image, (b-f) EDS elemental mapping of (b) La, (c) Sr, (d) Ga, (e) O and (f) F elements for the surface of $La_{1.5}Sr_{0.5}Ga_3O_{7.25-0.5\delta}F_\delta$ ceramic.

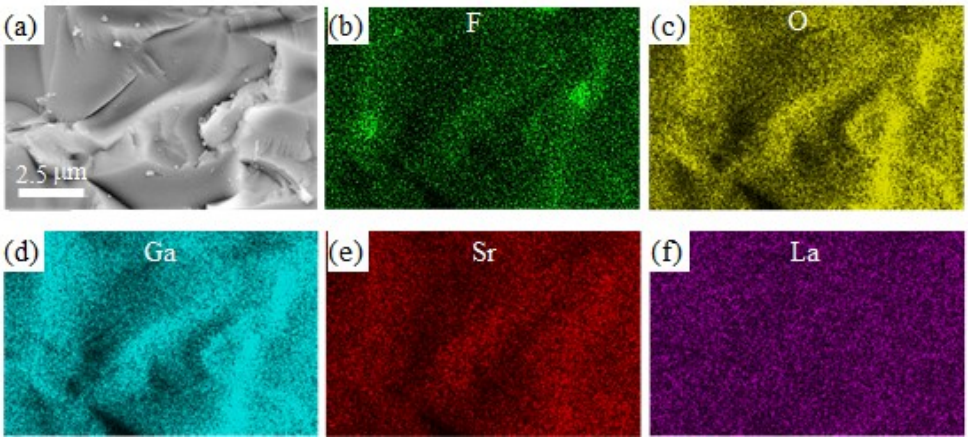

Figure S2. (a) SEM image, (b-f) EDS elemental mapping of (b) La, (c) Sr, (d) Ga, (e) O and (f) F elements for the cross-section of $La_{1.5}Sr_{0.5}Ga_3O_{7.25-0.5\delta}F_\delta$ ceramic. The uneven brightness is ascribed to the height variation over the examined area.

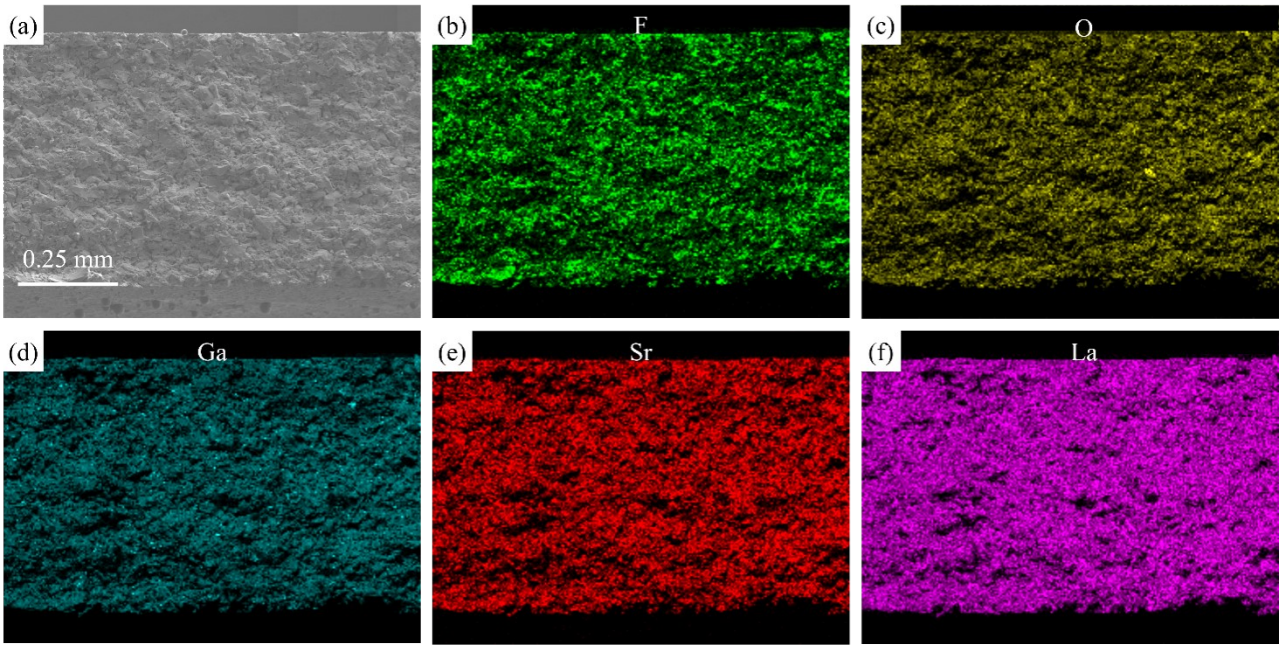

Figure S3. (a) SEM image, (b-f) EDS elemental mapping of (b) La, (c) Sr, (d) Ga, (e) O and (f) F elements for the cross-section of $La_{1.5}Sr_{0.5}Ga_3O_{7.25-0.5\delta}F_\delta$ ceramic.

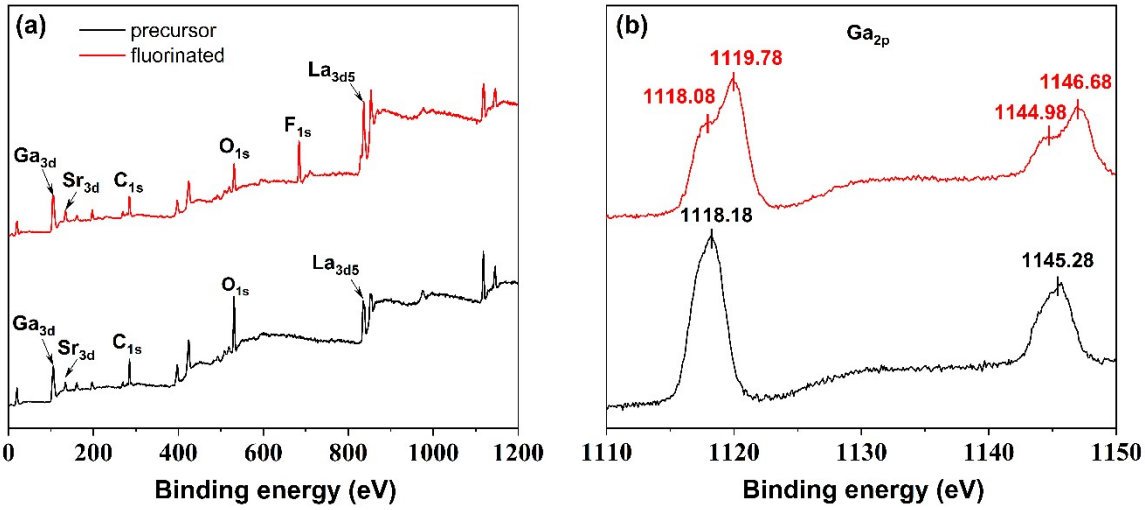

Figure S4. (a) XPS survey spectrum and (b) the Ga 2*p* peaks for fluorinated $La_{1.5}Sr_{0.5}Ga_3O_{7.25-0.5\delta}F_\delta$ and its precursor $La_{1.5}Sr_{0.5}Ga_3O_{7.25}$.

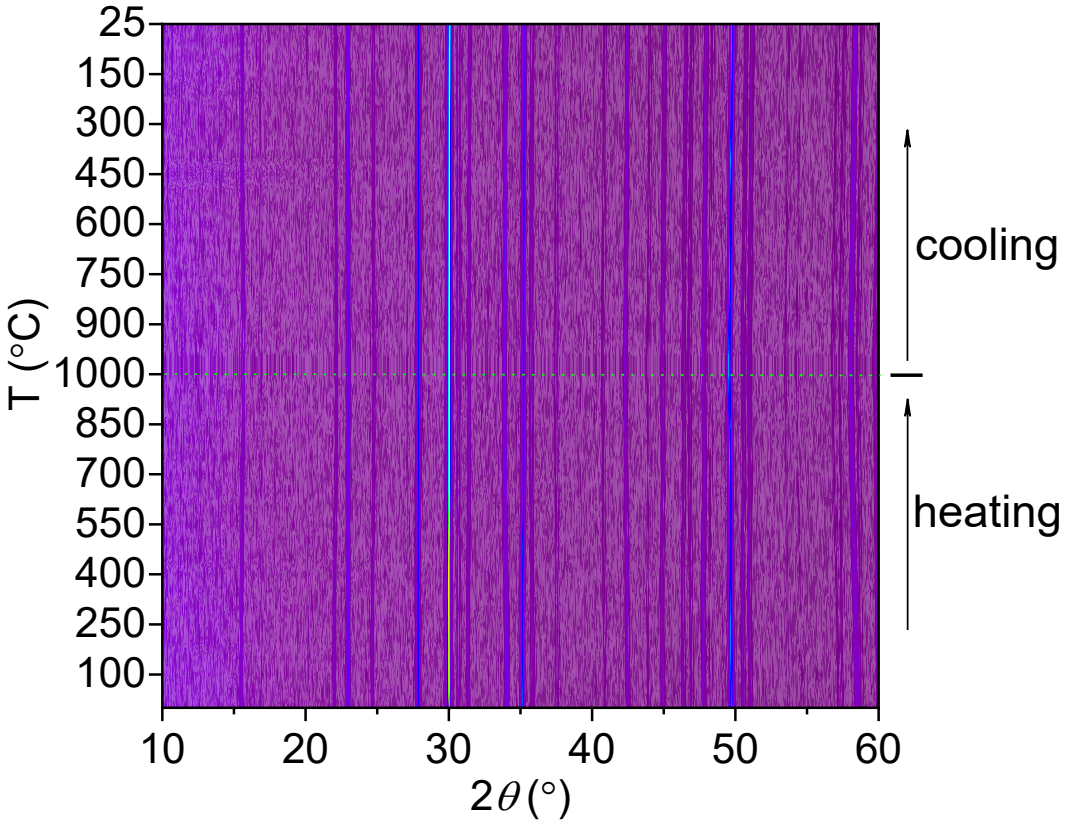

Figure S5. Film plots' of in situ VT-XRD patterns for fluorinated $La_{1.5}Sr_{0.5}Ga_3O_{7.25-0.5\delta}F_\delta$ powder within 25–1000 °C on heating and cooling process under vacuum atmosphere.

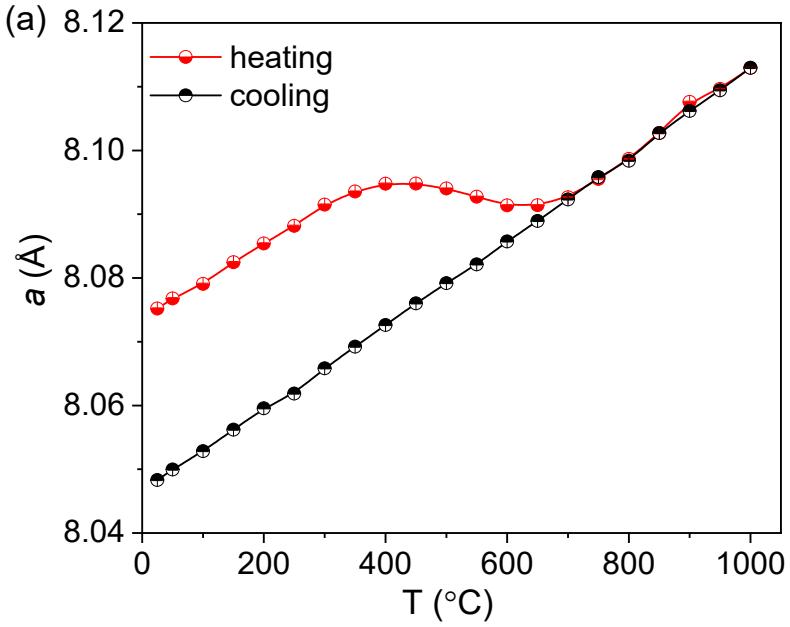

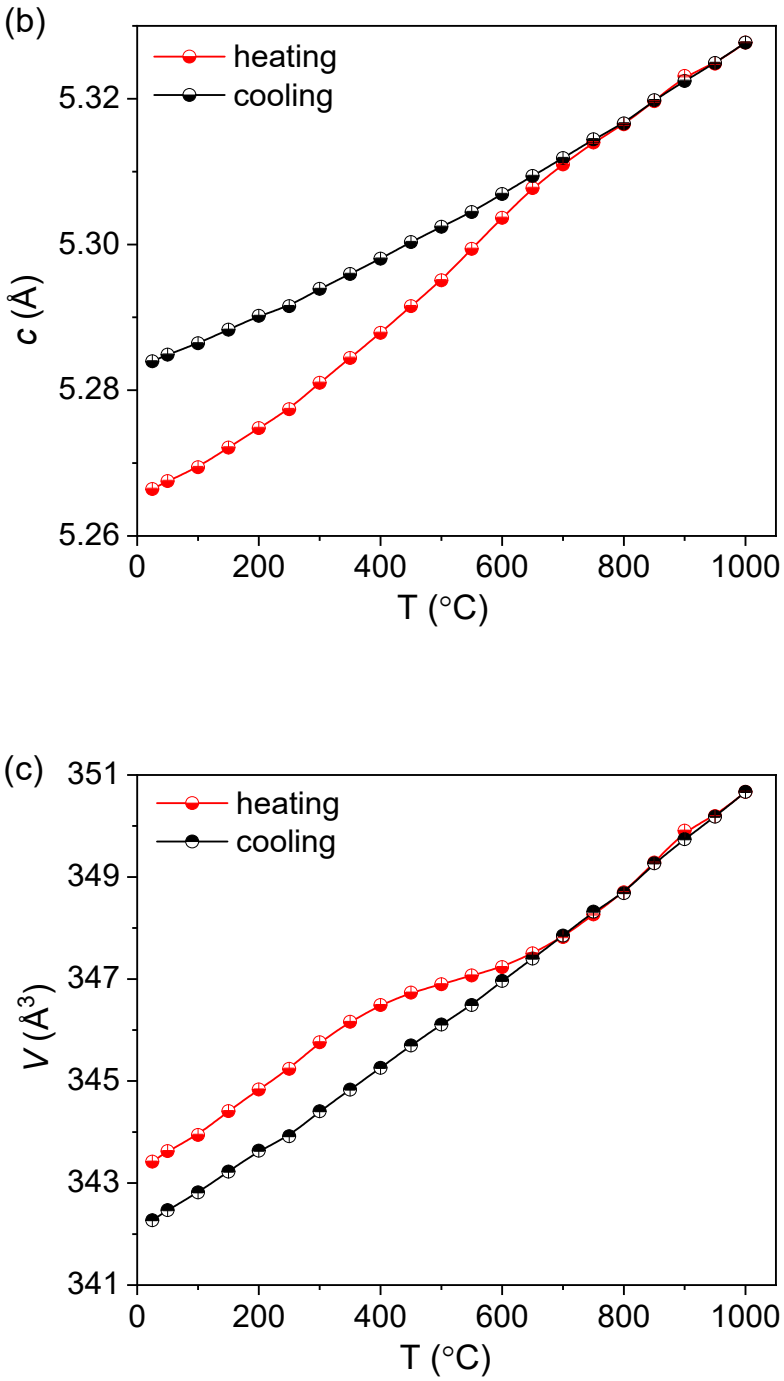

Figure S6. Temperature dependence of the refined cell parameters *a*, *c* and V for fluorinated $La_{1.5}Sr_{0.5}Ga_3O_{7.25-0.5\delta}F_\delta$ samples on heating and cooling process under vacuum atmosphere, corresponding to the VT-XRD measurement conditions distinct from the air environment shown in Figure 2.

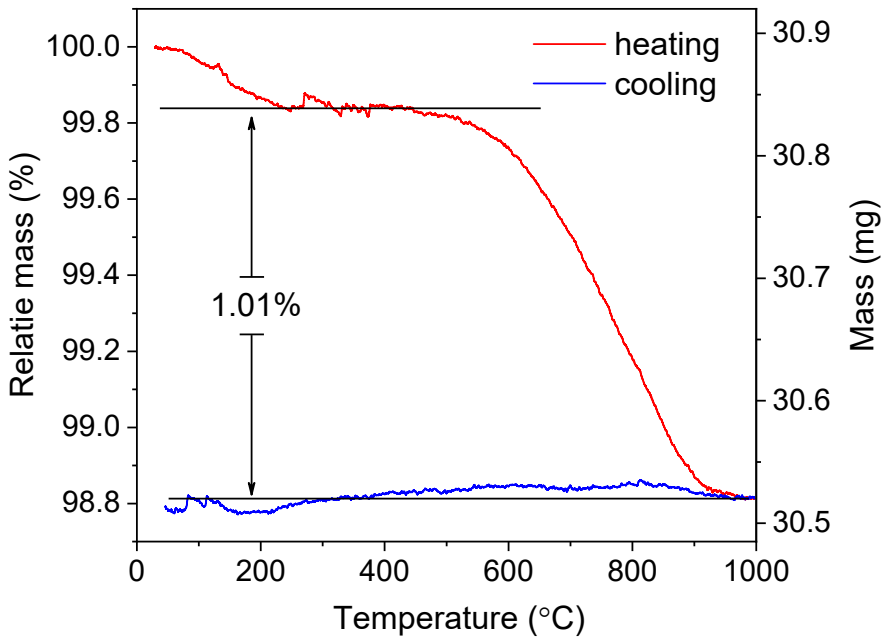

Figure S7. Thermogravimetric data under oxygen atmosphere of the $La_{1.5}Sr_{0.5}Ga_3O_{7.25-0.5\delta}F_\delta$ sample prepared from topotactic route.

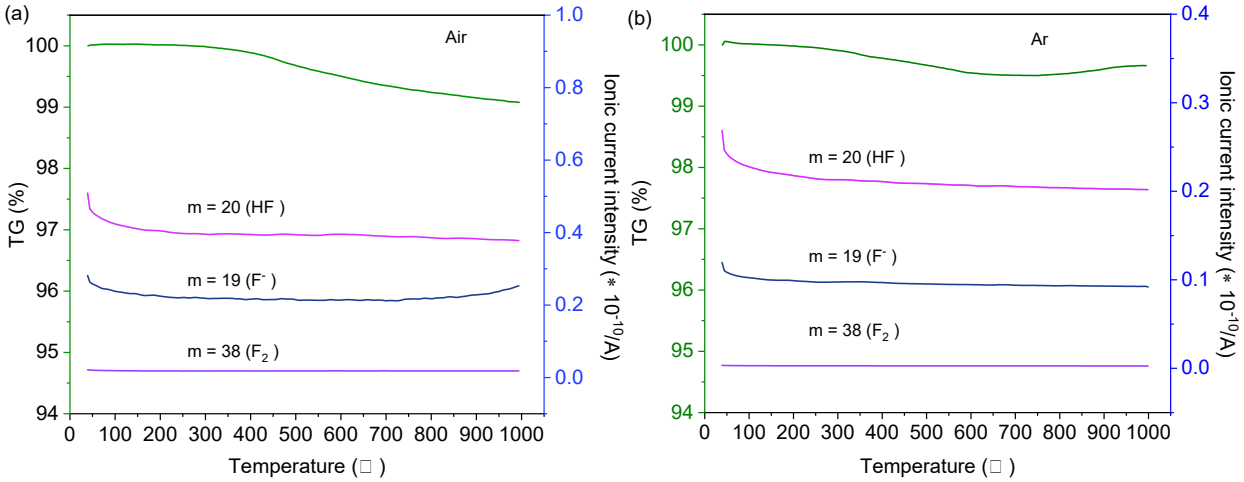

Figure S8. TG–MS curves of $La_{1.5}Sr_{0.5}Ga_3O_{7.25-0.5\delta}F_\delta$ measured in (a) air and (b) Ar atmospheres.

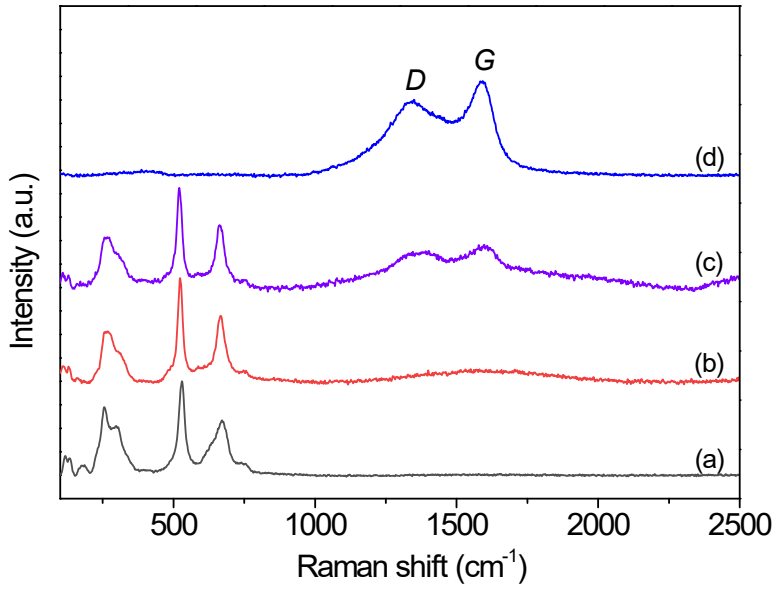

Figure S9. Raman spectra of (a) $La_{1.5}Sr_{0.5}Ga_3O_{7.25}$, (b) $La_{1.5}Sr_{0.5}Ga_3O_{7.25-0.5\delta}F_\delta$ containing trace residual decomposition products of PVDF, (c) $La_{1.5}Sr_{0.5}Ga_3O_{7.25-0.5\delta}F_\delta$ containing more residual decomposition products of PVDF and (d) the decomposition products of PVDF. *D* and *G* denote the presence of sp^3 and sp^2 hybridized carbon atoms, respectively.

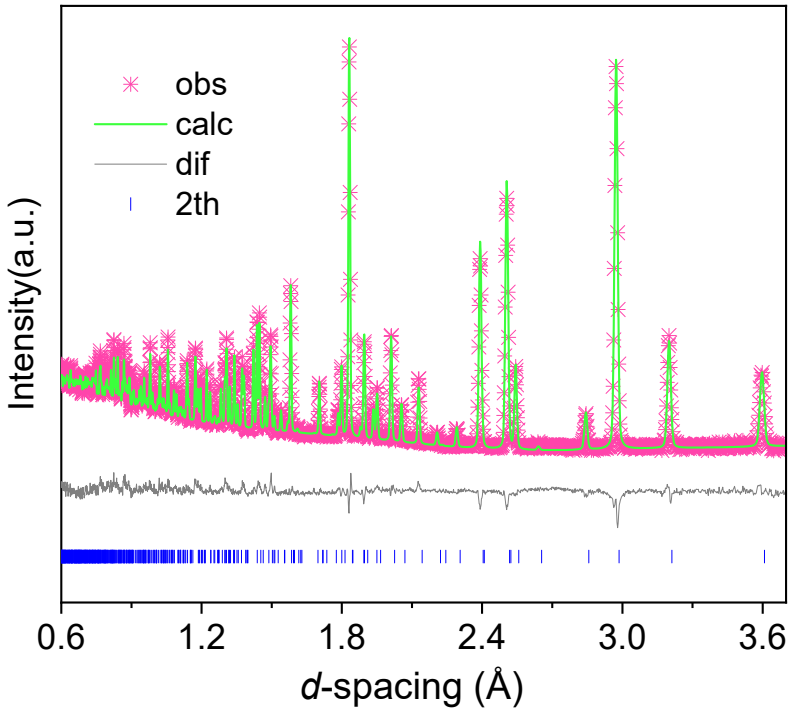

Figure S10. Rietveld refinement plots of NPD data for $La_{1.5}Sr_{0.5}Ga_3O_{7.25}$ powder. The reliability factors are R_{wp} ~ 2.76%, R_p ~ 2.30% and *GOF* ~ 1.39.

Table S1. (a) Refined fractional atomic coordinates and (b) anisotropic displacement parameters for $La_{1.5}Sr_{0.5}Ga_3O_{7.25}$*.

(a)	Site	*x*	*y*	*z*	occupancy
La/Sr	4*e*	0.3367(3)	0.1633(3)	0.5068(8)	0.75/0.25
Ga1	2*a*	0	0	0	1
Ga2	4*e*	0.1450(3)	0.3550(3)	0.9689(7)	1
O1	2*c*	0.5	0	0.190(1)	1
O2	4*e*	0.1372(4)	0.3628(4)	0.3158(6)	1
O3	8*f*	0.0846(5)	0.1628(5)	0.7923(6)	1
O4	4*e*	0.3319(7)	0.1681(7)	-0.009(7)	0.125

(b)	U_{11}(Å^2)	U_{22}(Å^2)	U_{33}(Å^2)	U_{12}(Å^2)	U_{13}(Å^2)	U_{23}(Å^2)
La/Sr	0.0076(8)	0.0076(8)	0.012(1)	0.003(1)	0.002(1)	-0.002(1)
Ga1	0.007(1)	0.007(1)	0.003(2)	0	0	0
Ga2	0.009(1)	0.009(1)	0.006(1)	-0.0001(7)	-0.001(4)	0.001(4)
O1	0.022(2)	0.022(2)	0.003(3)	-0.016(1)	0	0
O2	0.017(1)	0.017(1)	0.006(1)	0.002(2)	-0.001(1)	0.001(1)
O3	0.042(1)	0.011(1)	0.014(2)	-0.006(1)	0.013(1)	-0.006(1)
O4	0.031(5)	0.031(5)	0.040(5)	0.008(5)	-0.004(5)	0.004(5)

*Space group $P\bar{4}2_1m$, $Z = 2$, $a = b = 8.0224(1)$ Å, $c = 5.2685(1)$ Å, V = 339.07(1) Å^3.

Table S2. Bond lengths and bond valence sums (BVSs) for $La_{1.5}Sr_{0.5}Ga_3O_{7.25}$*.

Bond	Length (Å)	Bond	Length (Å)	Bond	Length (Å)
La/Sr-O1(×1)	2.494(3)	Ga1-O3(×4)	1.835(2)	O4-O1(×1)	2.176(2)
La/Sr-O2(×1)	2.478(3)	Ga1-O4(×4)*	2.98(3)	O4-O2(×1)	2.795(2)
La/Sr-O2(×2)	2.594(2)	$(BVS)_{Ga1}$	2.95	O4-O2(×2)	2.944(2)
La/Sr-O3(×2)	2.520(3)	Ga2-O1 (×1)	1.845(2)	O4-O3(×2)	2.243(2)
La/Sr-O3(×2)	2.896(3)	Ga2-O2(×1)	1.830(2)	O4-O3(×2)	2.694(2)
La/Sr-O4(×1) *	2.55(4)	Ga2-O3(×2)	1.864(2)	$(BVS)_{O1}$	2.37
La/Sr-O4(×1) *	2.72(4)	Ga2-O4(×2) *	2.53(5)	$(BVS)_{O2}$	1.75
$(BVS)_{La/Sr}$	2.55/2.21	Ga2-O4(×1) *	2.12(5)	$(BVS)_{O3}$	1.97
		$(BVS)_{Ga2}$	3.08	$(BVS)_{O4}$	1.08

* O4 site is partially occupied with occupancy 0.125.

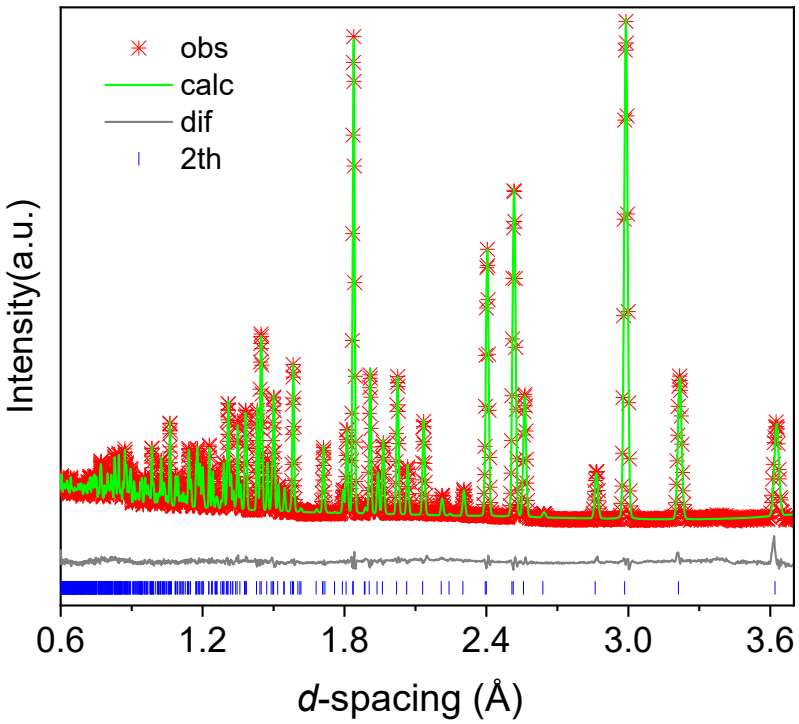

Figure S11. Rietveld refinement plots of NPD data for $La_{1.5}Sr_{0.5}Ga_3O_{7.25-0.5\delta}F_\delta$ sample using the average structure model assuming fluoride at both skeleton and interstitial oxygen sites. The reliability factors are R_{wp} ~ 3.16%, R_p ~ 3.08% and *GOF* ~ 1.36.

Table S3. Refined structural parameters for $La_{1.5}Sr_{0.5}Ga_3O_{7.25-0.5\delta}F_\delta$* at room temperature for the average structure model assuming fluoride at both skeleton and interstitial oxygen sites.

Atom	Site	*x*	*y*	*z*	occupancy
La/Sr	4*e*	0.3357(1)	0.1643(1)	0.5057(4)	0.75(3)/0.25(3)
Ga1	2*a*	0	0	0	1
Ga2	4*e*	0.1419(1)	0.3581(1)	0.9642(3)	1
O1/F1	2*c*	0	0	0.1922(8)	0.99(1)/0.01(1)
O2/F2	4*e*	0.1372(2)	0.3628(2)	0.3065(4)	0.999(1)/0.001(1)
O3/F3	8*f*	0.0819(2)	0.1650(2)	0.7946(4)	0.94(2)/0.06(2)
O4/ F4	4*e*	0.3344(1)	0.1656(1)	-0.003(1)	0.186(5)/0

* Space group $P\bar{4}2_1m$, $Z = 2$, $a = b = 8.0495(1)$ Å, $c = 5.2527(1)$ Å. $V = 340.35(1)$ Å^3.

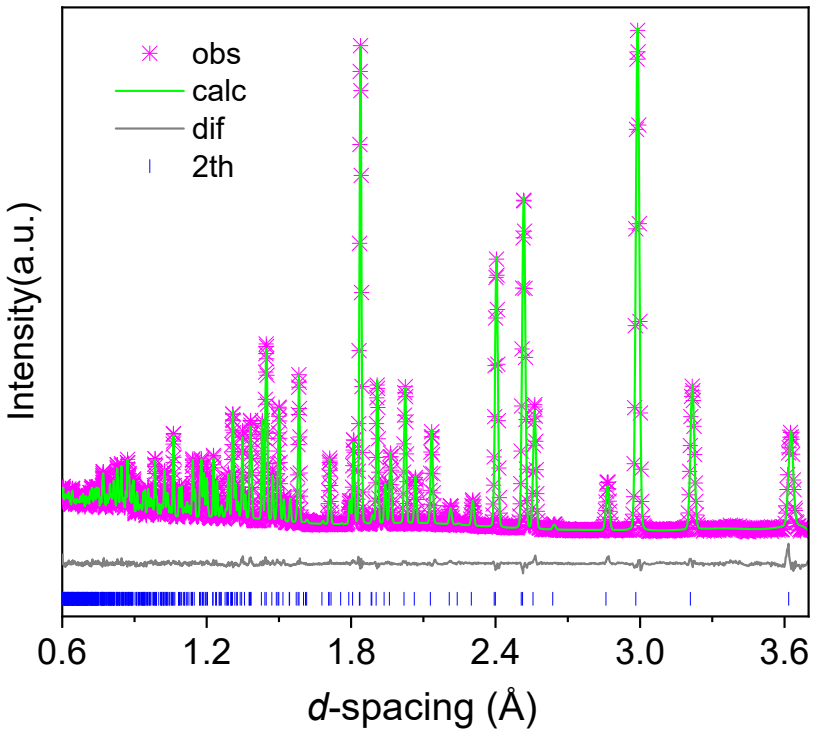

Figure S12. Rietveld refinement plots of NPD data for $La_{1.5}Sr_{0.5}Ga_3O_{7.25-0.5\delta}F_\delta$ sample using the average structure model with fluoride at the interstitial site only. The reliability factors are R_{wp} ~ 2.76%, R_p ~ 2.64% and *GOF* ~ 1.54.

Table S4. (a) Refined fractional atomic coordinates and (b) anisotropic displacement parameters for $La_{1.5}Sr_{0.5}Ga_3O_{7.25-0.5\delta}F_\delta$* with the average structure model with fluoride at the interstitial O4 site.

(a)	Site	*x*	*y*	*z*	occupancy
La/Sr	4*e*	0.3365(1)	0.1635(1)	0.5065(3)	0.75/0.25
Ga1	2*a*	0	0	0	1
Ga2	4*e*	0.1431(1)	0.3569(1)	0.9648(3)	1
O1	2*c*	0.5	0	0.1926(6)	1
O2	4*e*	0.1375(2)	0.3625(2)	0.3092(3)	1
O3	8*f*	0.0818(2)	0.1627(2)	0.7947(3)	1
O/F4	4*e*	0.3319(8)	0.1681(8)	-0.009(2)	0.05(3)/0.15(3)

(b)	U_{11}(Å^2)	U_{22}(Å^2)	U_{33}(Å^2)	U_{12}(Å^2)	U_{13}(Å^2)	U_{23}(Å^2)
La/Sr	0.0103(2)	0.0103(2)	0.0157(5)	0.0006(6)	-0.0010(5)	0.0010(5)
Ga1	0.0048(5)	0.0048 (5)	0.0061(9)	0	0	0
Ga2	0.0091(3)	0.0091(3)	0.0073(7)	-0.0001(7)	-0.0001(4)	0.0001(4)
O1	0.0187(7)	0.0187(7)	0.013(1)	-0.015(1)	0	0
O2	0.0173(5)	0.0173(5)	0.0109(7)	0.0024(9)	-0.0032(6)	0.0032(6)
O3	0.0281(7)	0.0181(6)	0.0221(7)	-0.0031(6)	0.0069(6)	-0.0023(6)
O/F4	0.015(2)	0.015(2)	0.005(3)	-0.005(4)	0.001(3)	-0.001(3)

*Space group $P\bar{4}2_1m$, $Z = 2$, $a = b$ =8.05466 (5) Å, c =5.25611 (5) Å, V = 341.003(5)Å^3.

Table S5. Bond lengths and bond valence sums (BVSs) for $La_{1.5}Sr_{0.5}Ga_3O_{7.133(3)}F_{0.267(6)}$* with the average structure model with fluoride at the interstitial site only.

Bond	Length (Å)	Bond	Length (Å)	Bond	Length (Å)
La/Sr-O1(×1)	2.488(9)	Ga1-O3(×4)	1.821(5)	O/F4-O1(×1)	2.18(3)
La/Sr-O2(×1)	2.493(8)	Ga1-O/F4(×4)*	2.99(1)	O/F4-O2(×1)	2.78(3)
La/Sr-O2(×2)	2.619(6)	$(BVS)_{Ga1}$	2.90	O/F4-O2(×2)	2.93(3)
La/Sr-O3(×2)	2.550(7)	Ga2-O1 (×1)	1.827(6)	O/F4-O3(×2)	2.26(3)
La/Sr-O3(×2)	2.894(6)	Ga2-O2(×1)	1.811(8)	O/F4-O3(×2)	2.68(1)
La/Sr-O/F4(×1) *	2.55(3)	Ga2-O3(×2)	1.868(6)	$(BVS)_{O1}$	2.37
La/Sr-O/F4(×1) *	2.71(3)	Ga2-O/F4(×2) *	2.52(2)	$(BVS)_{O2}$	1.71
$(BVS)_{La/Sr}$	2.53/2.19	Ga2-O/F4(×1) *	2.15(3)	$(BVS)_{O3}$	1.94
		$(BVS)_{Ga2}$	3.02	$(BVS)_{O/F4}$	1.10/0.66

* O/F4 site is partially occupied with 0.05 oxide ion and 0.15 fluoride ion, respectively.

Table S6. Bond angles in the GaO_n polyhedral for $La_{1.5}Sr_{0.5}Ga_3O_{7.25}$ and Bond angles in the $Ga(O/F)_n$ polyhedral $La_{1.5}Sr_{0.5}Ga_3O_{7.133(3)}F_{0.267(6)}$, respectively.

$La_{1.5}Sr_{0.5}Ga_3O_{7.25}$		$La_{1.5}Sr_{0.5}Ga_3O_{7.133(3)}F_{0.267(6)}$	
Bond	angles (°)	Bond	angles (°)
Ga1O4 tetrahedron		Ga1O4 tetrahedron	
O3-Ga1-O3(×4)	110.8(1)	O3-Ga1-O3(×4)	110.5(1)
O3-Ga1-O3(×2)	106.8(1)	O3-Ga1-O3(×2)	107.4(1)
Ga2O5 trigonal bipyramid		Ga2(O/F)5 trigonal bipyramid	
O1-Ga1-O2(×1)	114.2(1)	O1-Ga1-O2(×1)	114.9(2)
O1-Ga2-O3(×2)	97.5(1)	O1-Ga2-O3(×2)	98.3(1)
O1-Ga2-O4(×1)	156.2(1)	O1-Ga2-O/F4 (×1)	156.7(1)
O2-Ga2-O3(×2)	121.2(1)	O2-Ga2-O3(×2)	119.5(1)
O2-Ga2-O4(×1)	89.6(1)	O2-Ga2-O/F4(×1)	88.3(3)
O3-Ga2-O4 (×2)	68.1(1)	O3-Ga2-O/F4(×2)	68.0(2)

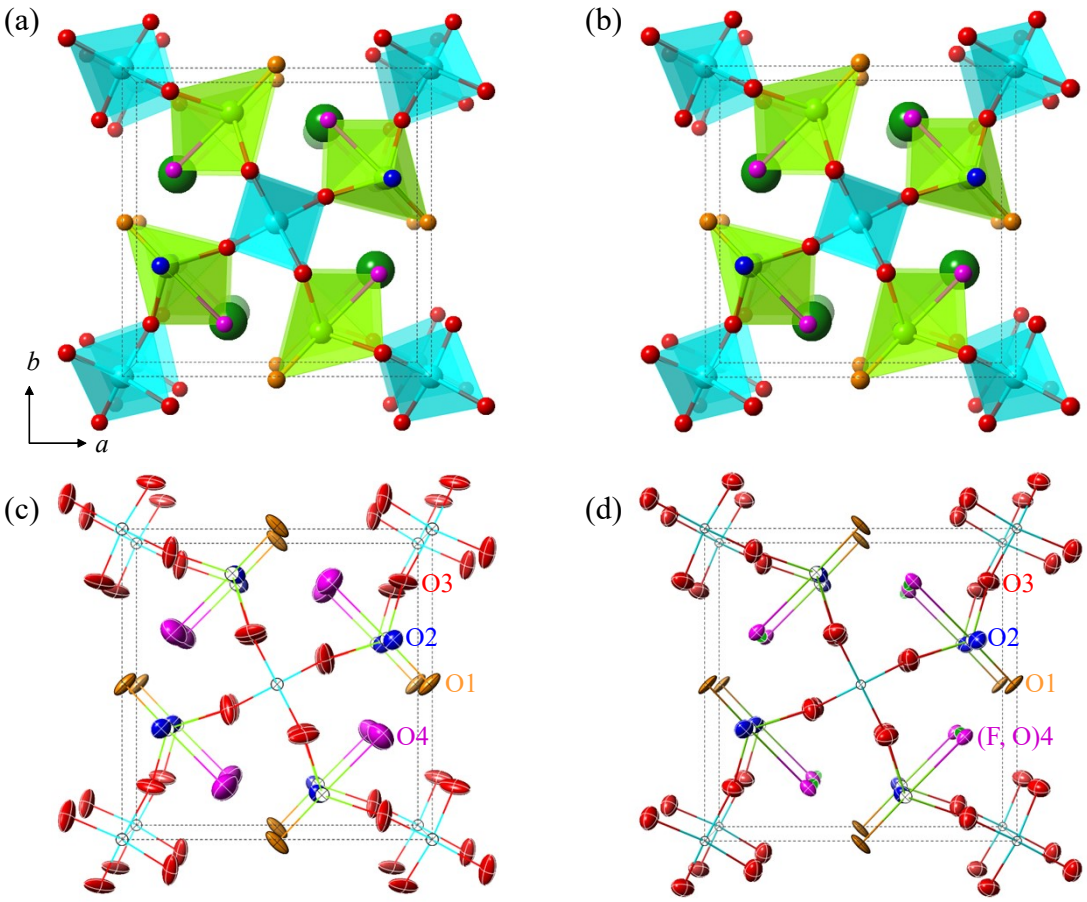

Figure S13. View along *c* axis of the refined structure for (a, c) $La_{1.5}Sr_{0.5}Ga_3O_{7.25}$ and (b, d) $La_{1.5}Sr_{0.5}Ga_3O_{7.133(3)}F_{0.267(6)}$ highlighting (a-b) the $Ga(O, F)_n$ polyhedral units and (c-d) the thermal ellipsoids (~70% probability level) of anionic atoms.

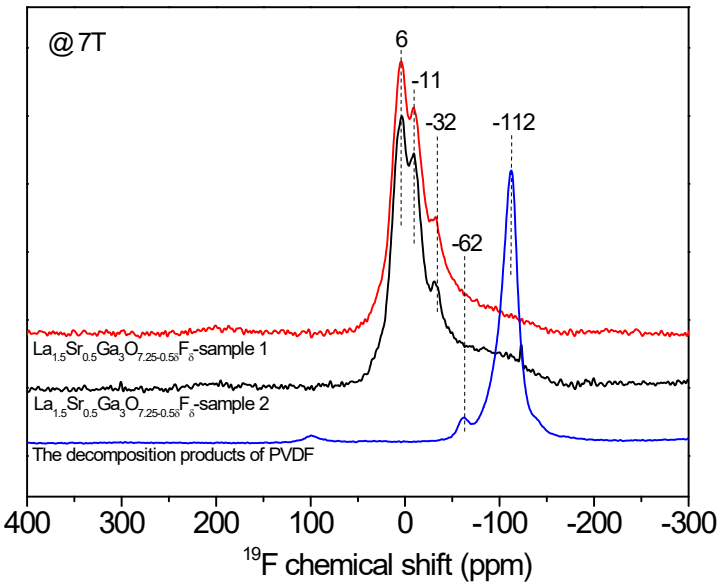

Figure S14. ^{19}F MAS NMR spectra of two $La_{1.5}Sr_{0.5}Ga_3O_{7.25-0.5\delta}F_\delta$ samples and the decomposition products of PVDF. For the two $La_{1.5}Sr_{0.5}Ga_3O_{7.25-0.5\delta}F_\delta$ samples, sample 1 contains trace of the residual decomposition products of PVDF, while sample 2 contains more residual decomposition products of PVDF.

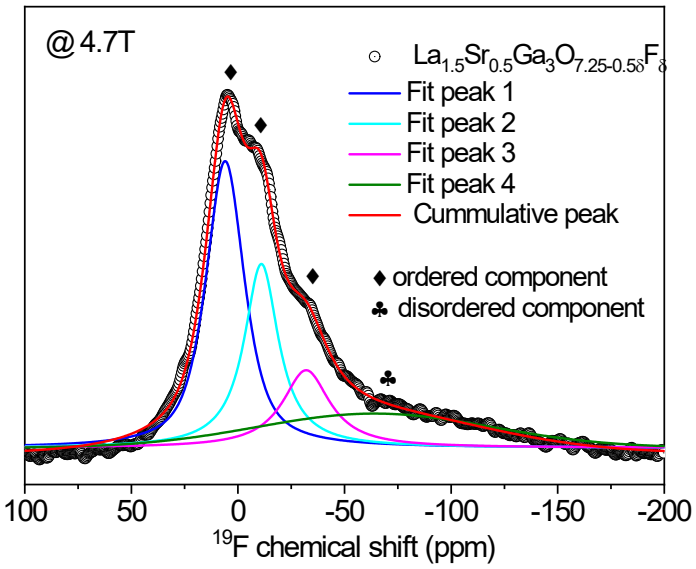

Figure S15. Deconvolution of NMR spectra for the $La_{1.5}Sr_{0.5}Ga_3O_{7.25-0.5\delta}F_\delta$ samples with traces of the residual decomposition products of PVDF under 4.7 T magnetic field.

Table S7. Fitted ^{19}F NMR chemical shifts δ_{iso} and relative intensities of $La_{1.5}Sr_{0.5}Ga_3O_{7.25-0.5\delta}F_{\delta}$ sample under 4.7 T and 7 T, respectively

Peak number	$_{iso}$ at 4.7 T MAS (ppm±1)	Relative intensities (%±2)	δ_{iso} at 7T MAS (ppm±1)	Relative intensities (%±2)
Peak 1	6	39	5.6	40
Peak 2	-11	25	-11.4	27
Peak 3	-32	14	-32.7	13
Peak 4	-64	22	-64.4	20

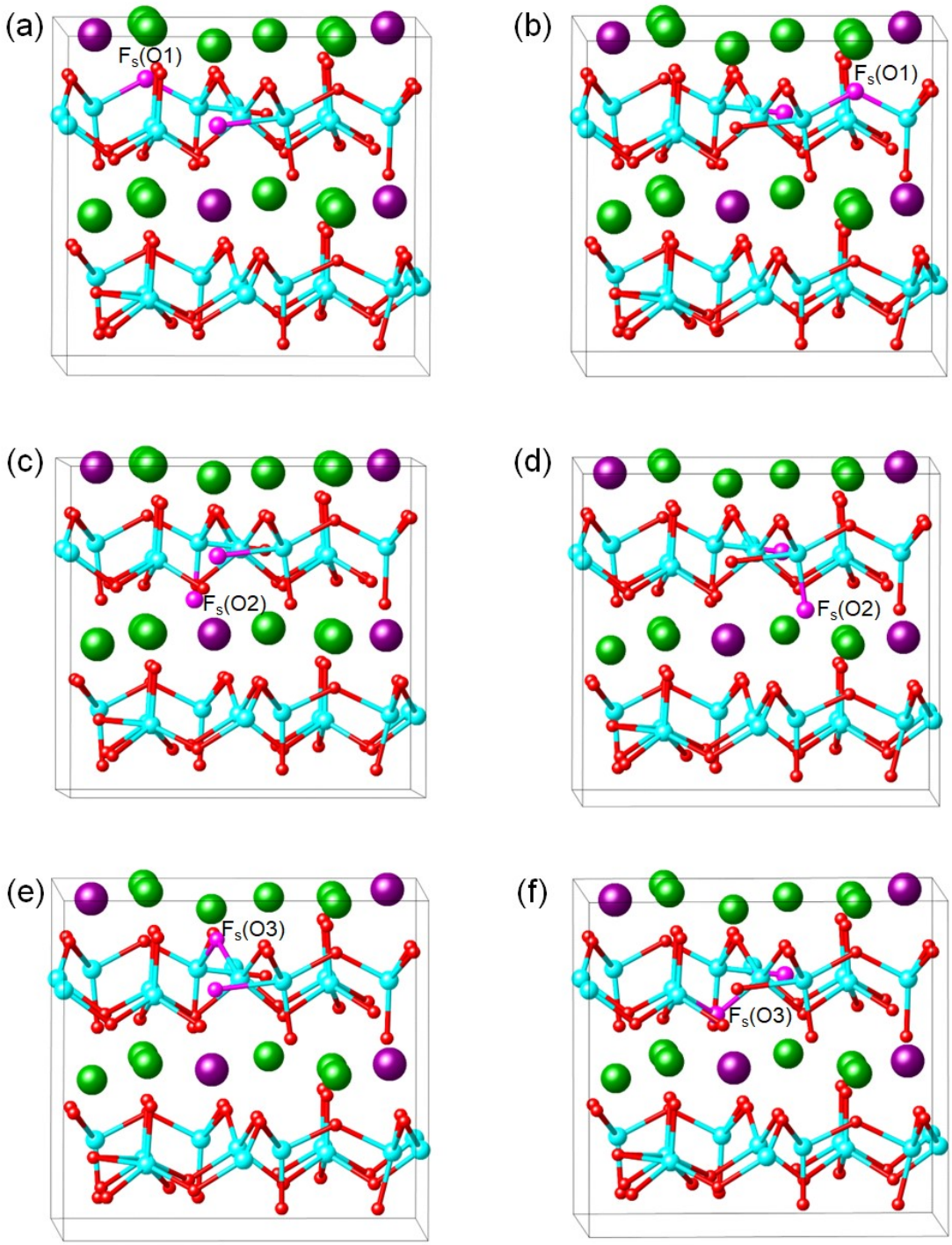

Figure S16. Local distribution of F on three different skeleton O sites in $La_{12}Sr_4Ga_{24}O_{57}F_2$ structure: (a-b) for O1 site, (c-d) for O2 and (e-f) for O3 sites. Medium green, violet, cyan, red and magenta spheres denote La, Sr, Ga, O and F atoms, respectively.

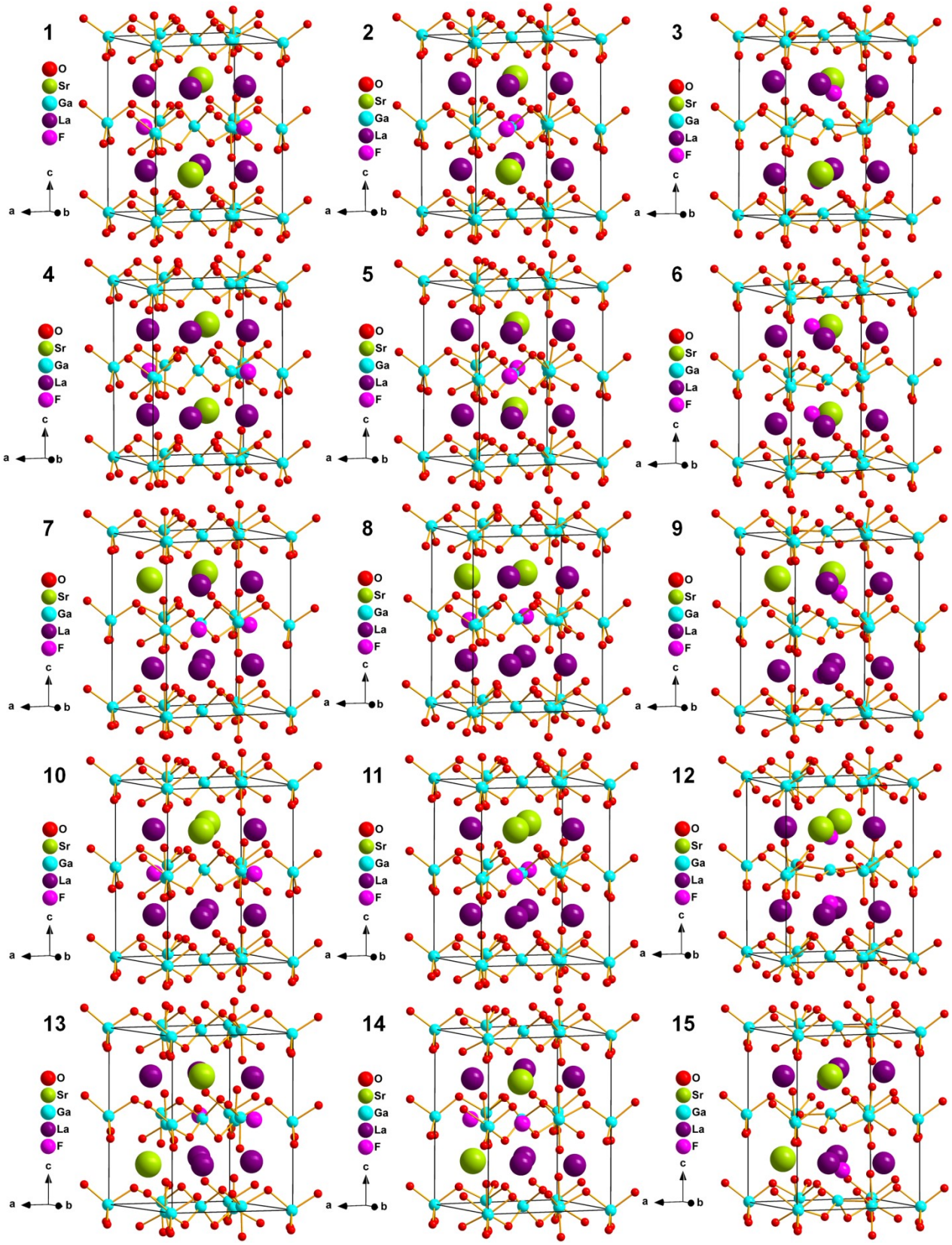

Figure S17. Fifteen possible configurations in $La_{1.5}Sr_{0.5}Ga_3O_7F_{0.5}$ highlighting the fluorine on interstitial oxygen sites.

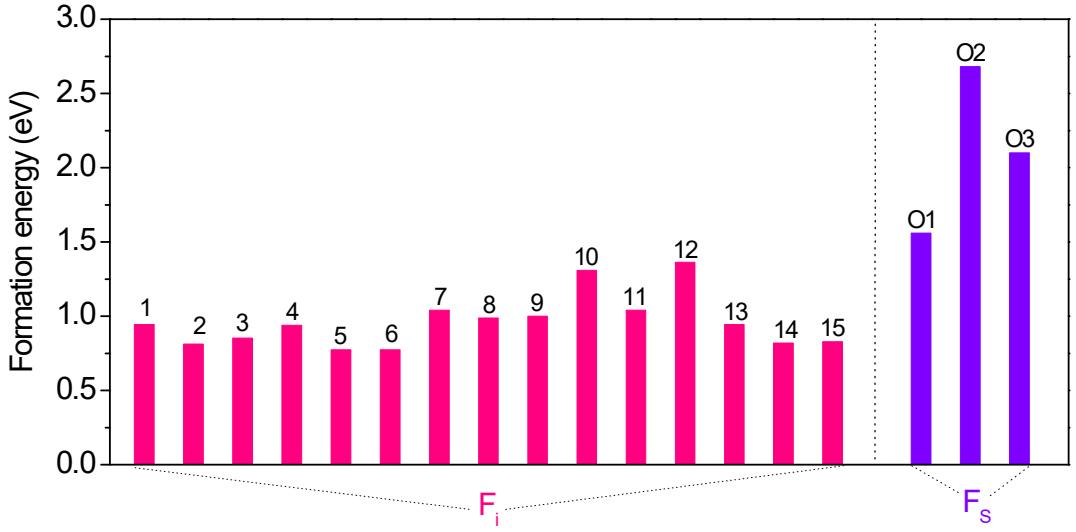

Figure S18. Comparison of the fluorine defects formation energies at fifteen interstitial sites (F_i) and three skeleton oxygen sites (Fs) in $La_{1.5}Sr_{0.5}Ga_3O_7F_{0.5}$ structure.

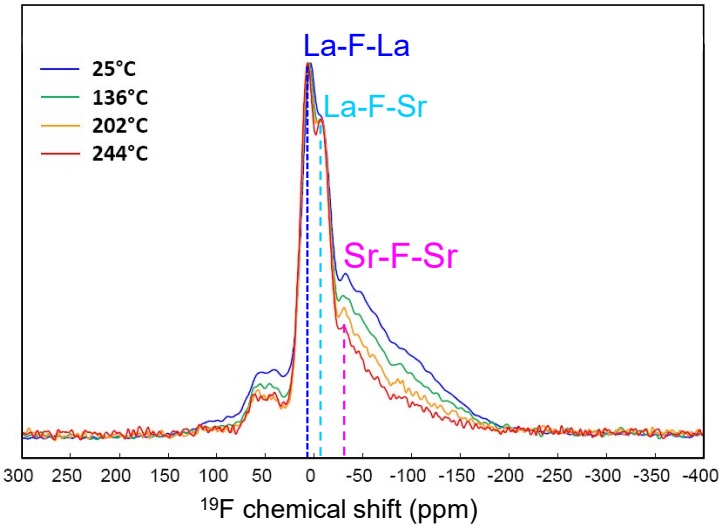

Figure S19. Variable-temperature ^{19}F MAS-NMR spectra of $La_{1.5}Sr_{0.5}Ga_3O_{7.25-0.5\delta}F_{\delta}$.

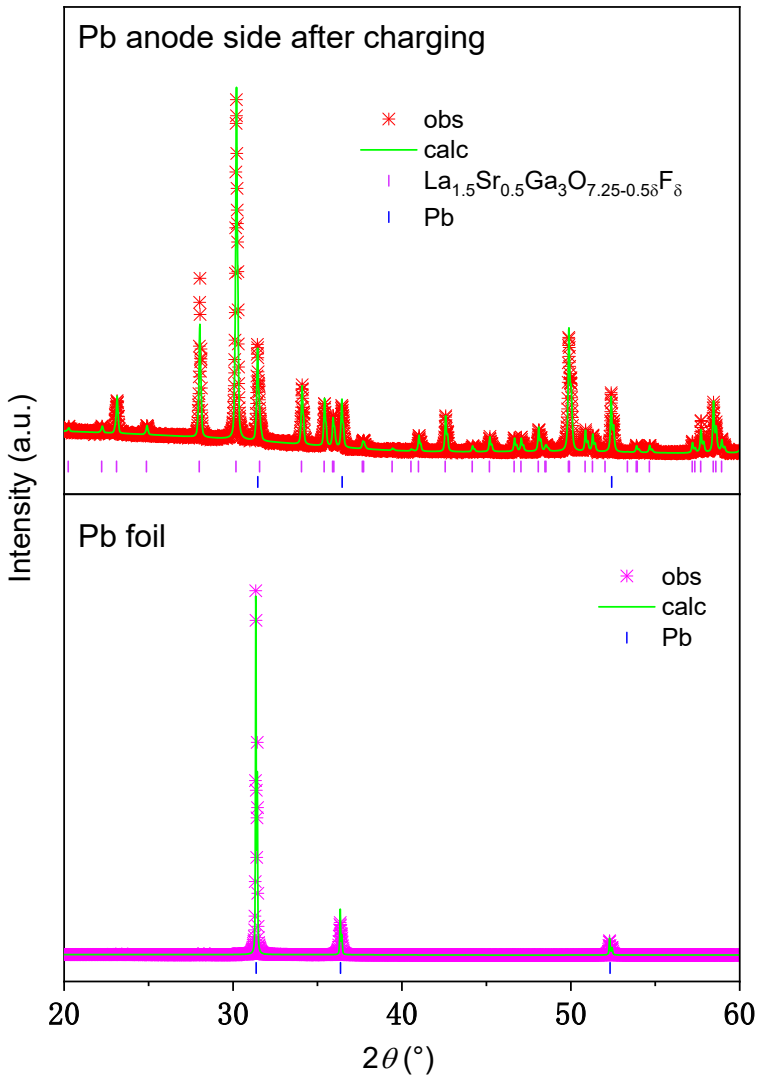

Figure S20. XRD patterns of Pb anode side after charging of the assemble fluoride-ion Swagelok cell compared to the XRD pattern of Pb foil.

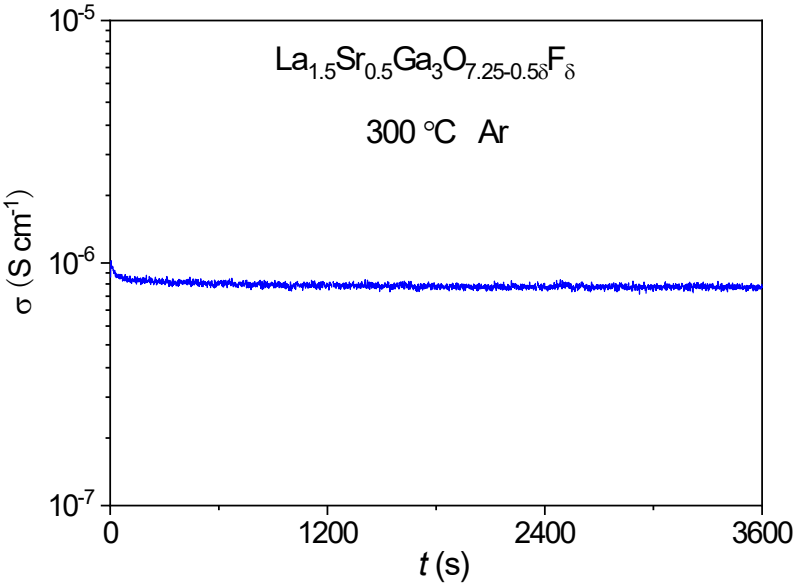

Figure S21. The potentiostatic direct-current measurement at 300 ℃ under Ar atmosphere for $La_{1.5}Sr_{0.5}Ga_3O_{7.25-0.5\delta}F_\delta$ for separating the electron contribution to total conductivity.

Supplementary Note. EMF measurements for $La_{1.5}Sr_{0.5}Ga_3O_{7.25-0.5\delta}F_\delta$.

Figure S18 shows the diagram of concentration cell for EMF measurements on oxygen transport numbers. The measured oxygen transport numbers of $La_{1.5}Sr_{0.5}Ga_3O_{7.25}$ and $La_{1.5}Sr_{0.5}Ga_3O_{7.25-0.5\delta}F_\delta$ up to 600 ℃ are shown in **Figure S19**. The EMF values for $La_{1.5}Sr_{0.5}Ga_3O_{7.25}$ below 500 ℃ on heating were not recorded successfully due to the poor gas tightness at low temperature. The gas tightness became good when the cell was warmed up to 500 ℃ and reasonable oxygen transport numbers were obtained. It is shown that the $t_{O^{2-}}$ value of $La_{1.5}Sr_{0.5}Ga_3O_{7.25}$ oxide pellet increase gradually from 0.5 to 0.96 as measured temperature rises. As well known to us, the interstitial oxygen-based melilite *c.a.* $La_{1.54}Sr_{0.46}Ga_3O_{7.27}$ is pure oxide ion conductors and features $t_{O^{2-}}$ ~ 0.9–0.95, for which the EMF measurements were carried out within 600-1000 °C (*Nat. Mater.* **2008**, *7*, 498–504). Here $La_{1.5}Sr_{0.5}Ga_3O_{7.25}$ displayed high oxygen transport numbers of 0.90-0.96 at 550°C and 600 °C, consistent with the previous results, but much lower oxygen transport numbers from 0.76 to 0.50 at low temperatures ≤ 500 ℃ on both heating and cooling. It is not surprising that $La_{1.5}Sr_{0.5}Ga_3O_{7.25}$ exhibited $t_{O^{2-}}$ value not higher than 0.9 until the temperature went to 500 ℃, then featured the characteristics of pure oxide ion conductors with an oxygen transport number of ~0.9–0.96 within 550–600 ℃. This is more probably attributed to less accuracy of the measured data at low temperatures ≤ 500 ℃ when the oxide ion migration is not so active. The reproducible lower oxygen transport numbers on cooling at low temperatures ≤ 500 ℃ may exclude the effect of gas tightness given the cell sealing went through the high temperature firing and stable oxygen transport numbers were obtained on heating and cooling within 550–600 ℃. Such less accuracies in the EMF measurements have been frequently seen in the commercial YSZ sensors.

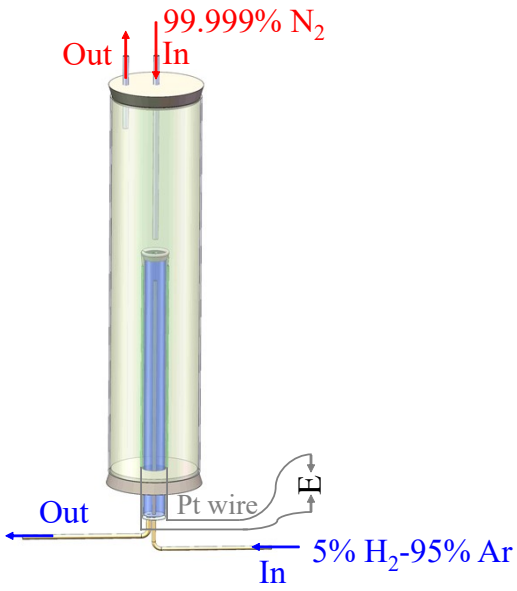

Figure S22. Diagram for the electromotive force measurements based on a concentration cell under $N_2||$ 5% H_2-95% Ar condition.

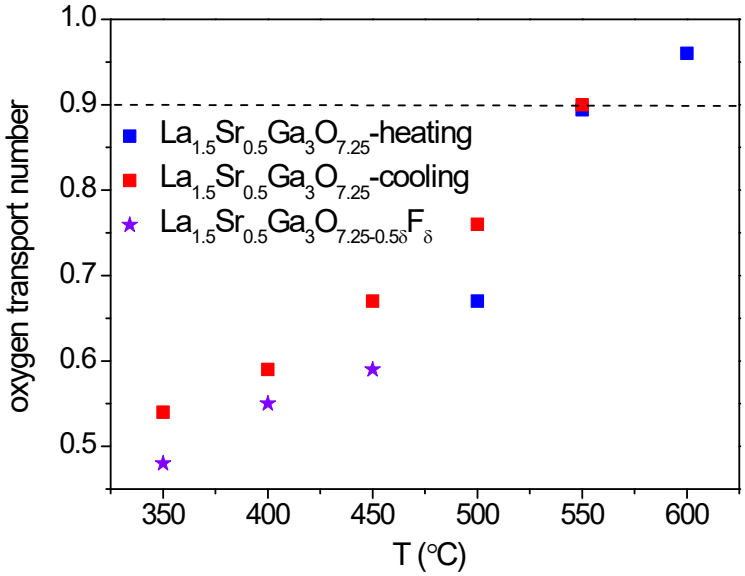

Figure S23. Oxygen transport numbers of $La_{1.5}Sr_{0.5}Ga_3O_{7.25}$ oxide and $La_{1.5}Sr_{0.5}Ga_3O_{7.25-0.5\delta}F_\delta$ oxyfluoride pellet up to 600 °C from the $N_2||$ 5% H_2-95% Ar concentration cells.

Considering the structure instability issue of the fluorinated samples based on the VTXRD and TG analysis (**Figure 2** and **Figure S4-6**), the oxygen transport numbers of $La_{1.5}Sr_{0.5}Ga_3O_{7.25-0.5\delta}F_\delta$

were only recorded within 350–450 ℃ temperature ranges on heating to avoid oxidation. Most of measurements were not successful due to the gas tightness problem at low temperature. Fortunately, reasonable sealing was still achieved on few cases, leading $t_{O^{2-}}$ values of ~0.48–0.59, slightly lower than those of $La_{1.5}Sr_{0.5}Ga_3O_{7.25}$ oxide. This indicates that oxide ions are the dominant carriers in the oxyfluoride materials but with small amount of contribution from electron conduction (**Figure S21**).